Journal of Statistical Physics, Vol. 75, Nos. 3/4, 1994

Periodic Orbit Expansions for the Lorentz Gas

Gary P. Morriss[1] and Lamberto Rondoni[1]

Received October 18, 1993; final December 23, 1993

We apply the periodic orbit expansion to the calculation of transport, thermodynamic, and chaotic properties of the finite-horizon triangular Lorentz gas. We show numerically that the inverse of the normalized Lyapunov number is a good estimate of the probability of an individual periodic orbit. We investigate the convergence of the periodic orbit expansion and compare it with the convergence of the cycle expansions obtained from the Ruelle dynamical ζ-function. For this system with severe pruning we find that applying standard convergence acceleration schemes to the periodic orbit expansion is superior to the dynamical ζ-function approach. The averages obtained from the periodic orbit expansion are within 8% of the values obtained from direct numerical time and ensemble averaging. None of the periodic orbit expansions used here is computationally competitive with the standard simulation approaches for calculating averages. However, we believe that these expansion methods are of fundamental importance, because they give a direct route to the phase space distribution function.

KEY WORDS: Symbolic dynamics; thermodynamics; Green–Kubo formulas; phase space.

1. INTRODUCTION

Recent works, such as the discovery that the conjugate pairing rule for the Lyapunov exponents of nonequilibrium systems[1] gives a direct connection between transport coefficients and nonlinear stability, and an equivalent result obtained by Gaspard and Rice,[2] have provided new reasons for studying model systems such as the Lorentz gas.[5–8] The Lorentz gas can be considered as a classical model for electrons moving independently through a crystal, and can be easily extended to simulate the motion under

[1] School of Physics, University of New South Wales, P.O. Box 1, Kensington NSW 2033, Australia. rondoni@newt.phys.unsw.edu.au.

0022-4715/94/0500-0553$07.00/0

an applied electric field. In nonequilibrium statistical mechanics, self-diffusion can be studied as the limiting case of mutual diffusion where the two species only differ in a *color* label,[9] and the smallest nontrivial system of this type contains two particles (one of each color).[4] This two-particle system in periodic boundary conditions is exactly equivalent to the Lorentz gas when the *color field* is zero, and its extension to nonzero fields leads to a more complicated dynamics for the wandering particle between collisions. The Lorentz gas is clearly one of the simplest deterministic systems[3,4] which exhibits diffusion in the absence of a field and a steady current away from equilibrium, and has therefore been recently reexamined[6] in an attempt to determine which microscopic dynamics yield classical transport.

There is an exact equivalence between the Hamiltonian for the equilibrium molecular dynamics simulation of two hard disks in two dimensions in periodic boundary conditions and the Hamiltonian for the modified Lorentz gas (the original Lorentz gas has random rather than regularly arranged scatterers). The equations of motion for the two hard disk system are

$$\dot{\mathbf{r}}_i = \frac{\mathbf{p}_i}{m} \qquad \text{and} \qquad \dot{\mathbf{p}}_i = \mathbf{F}_i \tag{1}$$

where $i = 1, 2$. The coordinate origin can be shifted to be the position of particle 1 by moving to relative coordinates $\mathbf{r} = \mathbf{r}_2 - \mathbf{r}_1$ and $\mathbf{p} = \mathbf{p}_2 - \mathbf{p}_1$. Defining the force in relative coordinates to be $\mathbf{F} = \mathbf{F}_2 - \mathbf{F}_1 = 2\mathbf{F}_2$, we obtain the same equations of motion as before, with the subscripts removed. As the force is only nonzero when particles 1 and 2 are in contact (that is, the centers are separated by the particle diameter σ), the size of particle 1 and all its periodic images can be expanded so their new diameter is 2σ, and the diameter of particle 2 reduced to zero. It is easy to see that the motion of particle 2 is now that of a point particle *wandering* through a regular lattice of scatterers (particle 1 and its periodic images). The periodicity of the lattice is the same as that of the periodic boundary conditions. The constraint of either constant energy or constant kinetic energy for a two-particle system implies that the speed of the wandering particle (particle 2) must be constant. For the usual cubic periodic boundary conditions the wandering point particle always has an infinite horizon (that is, for special initial conditions it can pass through the whole lattice without a collision). To avoid the subsequent difficulties with the definition of the diffusion coefficient we adopt a triangular lattice, and we choose the density sufficiently large so that the horizon is finite. As the speed of the wandering particle is constant, the momentum has only one degree of freedom, its direction, so we can write $\mathbf{p} = p(\cos\theta, \sin\theta)$, where θ is the

angle between the x axis and the momentum vector. The equations of motion for the wandering particle between collisions are

$$\dot{x} = \frac{p}{m}\cos\theta, \qquad \dot{y} = \frac{p}{m}\sin\theta, \qquad \dot{\theta} = 0 \tag{2}$$

Integrated, these equations give straight-line trajectories. It is sometimes more convenient to represent the position in polar coordinates, so that $(x, y) = r(\cos\phi, \sin\phi)$ (Fig. 1).

Machta and Zwanzig[3] have characterized the thermodynamic state point of the Lorentz gas in terms of the disk spacing w, so if d is the distance between the centers, then $w = d - 2\sigma$. In what follows we take $\sigma = 1$, and it is straightforward to show that the density of the infinitely periodic two-particle system is related to the spacing in the Lorentz gas by the relation

$$\rho = \frac{1}{\sqrt{3}}\left(\frac{2}{w+2}\right)^2$$

For a finite horizon we require that $0 \leqslant w \leqslant 4/\sqrt{3} - 2$. See Section 4 for more details.

This paper is organized as follows. In Section 2 we present some new bounds on the value of the diffusion coefficient and the pressure for the periodic Lorentz gas, obtained from direct numerical simulations for a range of spacings w. In Section 3 we discuss the recently developed periodic orbit expansion method and its links with the calculation of thermodynamic quantities. In particular, we test the claim that these methods produce better results than the standard simulation methods. Sections 4 and 5 are devoted to the development of symbolic dynamics needed for periodic orbit studies of the Lorentz gas. Section 6 describes the numerical schemes used in our study. In Section 7 we present the numerical results

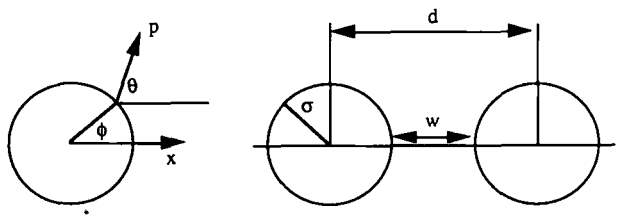

Fig. 1. The geometry of the Lorentz gas. For the scatterer at collision, the polar angle ϕ gives the position of the moving particle, while θ gives the angle between its momentum vector and the x axis. The state point can be represented by the density or by specifying the spacing between scatterers w.

obtained from the two different periodic orbit expansion methods, which we hereafter refer to as the *periodic orbit expansion*[7] and the *cycle expansion*,[8] and compare them with our direct simulation method estimates in Section 2. The conclusions of our study are summarized in Section 8.

2. DIFFUSION COEFFICIENT AND PRESSURE

There are a variety of direct simulation methods used to compute the diffusion coefficient D.[9] In this section we give the results of new numerical simulations of an ensemble of Lorentz gas systems uniformly distributed in the part of phase space not occupied by the scatterer of the elementary cell of the triangular array described in Section 1. Here, by elementary cell (EC) we mean a hexagon whose replicas tile the whole two-dimensional plane. This hexagon is formed by the perpendicular bisectors of the lines joining the center of the central scatterer to the centers of the six nearest neighbor scatterers. Each initial condition in the EC is associated with a set of different momenta uniformly distributed to fill up the surface of the unit ball in momentum space. In our system there are no external forces, so the point particle travels with constant velocity between two collisions, and the mass and speed are taken to be one. This model is similar to the Lorentz gas of the previous section, the only difference being that instead of considering a single particle, we follow an ensemble of Lorentz gas systems and calculate averages over the ensemble as a function of time. In particular, we compare the values of D as obtained from the use of the Einstein relation and the Green–Kubo formula. As expected, both methods provide us with basically the same values of D, although the numerical efficiencies of the two methods are different. Note: every ensemble which can be modeled on a computer necessarily contains a finite number of elements. Thus, when we speak of ensemble averages we actually mean approximations of phase space integrals by means of finite sums.

To see how the Einstein and Green–Kubo formulas produce the same results we may argue as follows. Let us assume that the ensemble average of the mean square displacement $\langle \Delta \mathbf{r}(t)^2 \rangle$ grows linearly with t at large time. Then, the Einstein relation for D in three dimensions can be written as

$$D = \lim_{t \to \infty} \frac{1}{6} \frac{\langle \Delta \mathbf{r}(t)^2 \rangle}{t} = \lim_{t \to \infty} \frac{1}{6} \frac{d}{dt} \langle \Delta \mathbf{r}(t)^2 \rangle \tag{3}$$

where $\langle\ \rangle$ indicate an ensemble average, and the displacement of a single member of the ensemble is defined by

$$\Delta \mathbf{r}(t) = \mathbf{r}(t) - \mathbf{r}(0) = \int_0^t dt' \, \mathbf{v}(t')$$

So from Eq. (3), the diffusion coefficient can be written as

$$D = \lim_{t \to \infty} \tfrac{1}{3} \langle \Delta \mathbf{r}(t) \cdot \mathbf{v}(t) \rangle = \lim_{t \to \infty} \int_0^t ds\, \tfrac{1}{3} \langle \mathbf{v}(s) \cdot \mathbf{v}(t) \rangle \tag{4}$$

which is similar to a Green–Kubo relation. In order to obtain precisely the Green–Kubo expression for D we have to use the properties of the equilibrium distribution function. In particular we require that, for any two phase variables, A and B say, the equilibrium-time correlation function only depends upon the time difference between the two phase variables, i.e.,

$$\langle A(t)\, B(0) \rangle = \langle A(0)\, B(-t) \rangle \tag{5}$$

This can be proved by moving the time evolution propagator from phase variable $A(t)\, B(0)$ to the distribution function, and it can be viewed as a consequence of the equivalence of Schrödinger and Heisenberg representations for time evolution under the classical Liouville operator.[9] After a simple change in variables, the diffusion coefficient becomes

$$D = \lim_{T \to \infty} \int_0^T dt'\, \tfrac{1}{3} \langle \mathbf{v}(0) \cdot \mathbf{v}(t') \rangle = \int_0^\infty dt'\, \tfrac{1}{3} \langle \mathbf{v}(0) \cdot \mathbf{v}(t') \rangle \tag{6}$$

which is the Green–Kubo relation for the diffusion coefficient. An identical argument applies to the two-dimensional system, where the factor 1/6 in Eq. (3) is replaced by 1/4. This proves the equivalence of the mean square displacement formula and the Green–Kubo relation. However, in a molecular dynamics calculation we always have a finite (rather than infinite) time and a finite number of ensemble members in the average.

The problem, now, is to find the best estimate of D by extrapolating to the limit of large times and large ensemble sizes. From the numerical point of view we can either fix the time interval T and extrapolate the ensemble size, or fix the number of ensemble members and extrapolate to infinite time T. We find that the mean square displacement converges quickly with increasing ensemble size, but slowly with increasing T. By contrast, the Green–Kubo integral converges quickly with increasing T, but slowly with increasing ensemble size. The computational technique that we use to get the best estimate of D in the limit (ensemble size, T) $\to \infty$ is to choose a sufficiently large value of the quickly convergent variable and then extrapolate the diffusion coefficient as a function of the inverse of the slow variable. In Fig. 2 we present the results obtained for $w = 0.3$. The Green–Kubo diffusion coefficient converges like a random variable with increasing ensemble size, while the mean square displacement is a

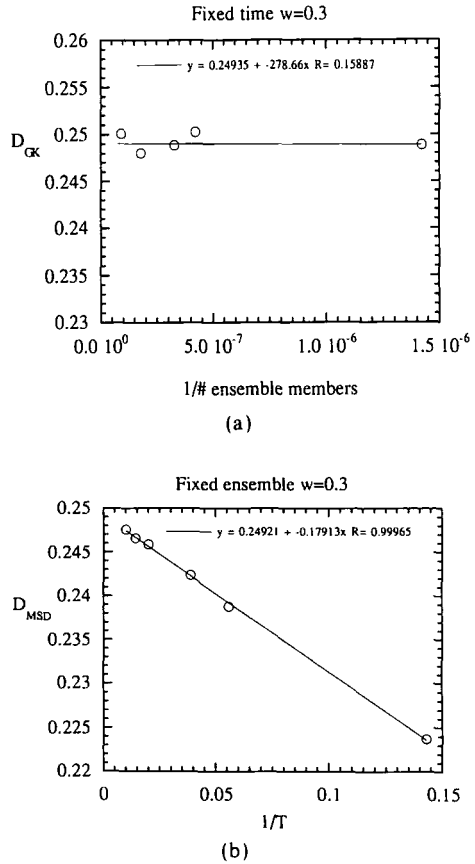

Fig. 2. (a) The extrapolation of the diffusion coefficient from the Green–Kubo formula D_{GK} versus the inverse of the number of ensemble members. The upper limit of the integral is fixed at $T = 17.9$. D_{GK} converges like a random variable to 0.24935. (b) The extrapolation of the diffusion coefficient from the mean-square displacement D_{MSD} versus the inverse of T. The number of ensemble members is fixed at 152,520. Here the convergence is almost exactly linear to a value of 0.24921. The consistency of the limiting values is most impressive.

monotonically increasing linear function of T. There is an impressive consistency between the two methods of calculating the diffusion coefficient.

Our simulations show that the assumption that $\langle \Delta \mathbf{r}(t)^2 \rangle$ grows linearly with time at large times is very well satisfied in the Lorentz gas for all the different values of w that we have considered. However, it is worth noting that such behavior is not observed when a single trajectory is simulated. Indeed, for closed loops (composed of many traversals of a single closed periodic orbit) $\Delta \mathbf{r}(t)^2$ is strictly bounded. Also, there are

trajectories which look periodic in the EC, but not in the full phase space, whose square displacement grows as t^2 in the limit of large times (the existence of orbits of this kind will be clarified in Section 4). Moreover, we always observe that a single generic chaotic trajectory has a square displacement which does not appear to approach linear growth, and that it is essential to consider ensembles to obtain linear growth in $\langle \Delta \mathbf{r}(t)^2 \rangle$ (this occurs despite the proved ergodicity of this system).

In Table I we compare our extrapolated results with those previously published in the literature. The column labeled D_{th} gives the approximate theoretical diffusion coefficient calculated by Machta and Zwanzig, while D_{MZ} is the Green–Kubo calculation by the same authors.[3] D_{esc} is the diffusion coefficient calculated by Gaspard and Baras using their escape rate method.[5] The column labeled D_{BEC} gives the results obtained by Baranyi *et al.*,[10] while the column labeled D^* gives the results obtained here from a combination of extrapolations of Green–Kubo and Einstein formulas. In the table the number in parentheses is the uncertainty in the last digit of the quoted result. It is interesting to note that the results in the column labeled D_{BEC}, which were obtained in a rather original way—that of extrapolating from soft-sphere potentials to hard-disk potential—are in very good agreement with our present results.

The instantaneous expression for the pressure tensor $\mathbf{P}(t)$ can be written as a function of the instantaneous values of position and momentum to obtain

$$\mathbf{P}V = \sum_{i=1}^{N} \frac{\mathbf{p}_i \mathbf{p}_i}{m} - \frac{1}{2} \sum_{i,j=1}^{N} \mathbf{r}_{ij} \mathbf{F}_{ij} \tag{7}$$

where V is the volume of the system, $\mathbf{F}_{ij}$ is zero except at a collision, and $\mathbf{p}_i$ is constant between two collisions. The average value of the pressure can be obtained to high accuracy by calculation of the time average of Eq. (7).[9] Due to the ergodicity of the system, the ensemble average and time average are equal. We calculated the average pressure for 31 values of

Table I. The Diffusion Coefficient

w	D_{th}	D_{MZ}	D_{esc}	D_{BEC}	D^*
0.10	0.104	0.10(1)	0.096(7)	0.098(5)	0.0995(3)
0.15	0.128	0.14(1)	0.134(4)	—	0.1350(5)
0.20	—	—	—	0.167(10)	0.170(1)
0.236	0.158	—	—	—	0.197(1)
0.30	0.175	0.25(1)	0.25(1)	0.247(8)	0.2492(3)

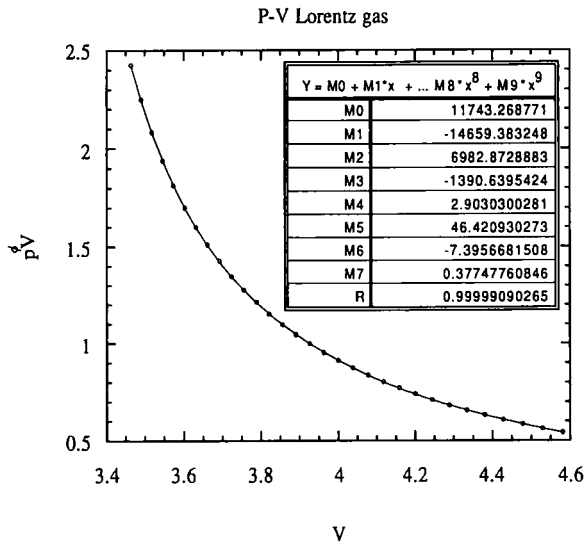

Fig. 3. The equation of state for the Lorentz gas. For the purpose of interpolating the equation of state it has been fitted to a ninth-order polynomial whose coefficients M0 to M9 are listed.

w in the range $[0, 0.3]$, and we found that simulation runs of 10^6 collisions were sufficient to obtain $\mathbf{P}$ with a precision of five or more significant figures. Our results are presented in Fig. 3, along with a polynomial fit whose accuracy is estimated by the factor R (an exact fit is $R = 1$). In this equilibrium system the pressure tensor is diagonal and the kinetic part is trivially related to the total kinetic energy. As a result we calculate only the nontrivial potential contribution to the trace of the pressure tensor divided by the dimension of the system p^{ϕ}. The volume of the system for a given w is computed from the expression $V = N/\rho = 2/\rho$, where the density ρ can be obtained from the spacing using the expression given in Section 1.

3. PERIODIC ORBIT EXPANSION

It has been noted in a large number of works from both the mathematical and the physical literature that the properties of many chaotic systems can be studied in terms of unstable periodic orbits (UPOs), and that the relevant attractors can be hierarchically approximated through sets of progressively longer and longer unstable periodic orbits.[7,8,11-17] In this approach, the UPOs are grouped into sets of prime ones, P_n say, with the same number n of collisions, where prime means that each member of

P_n undergoes exactly n collisions in a time equal to its own period. One attaches a stability weight to each particular UPO which is inversely proportional to the product of its expanding Lyapunov numbers Λ_i.[14] (The reason why such weights are related to the stability of UPOs is that a Lyapunov number can be viewed as a measure of the instability of the orbit with which it is associated, as it takes on larger values as the instability of the orbit increases.) In the two-dimensional Lorentz gas there is exactly one expanding Lyapunov number (or exactly one positive Lyapunov exponent). One of the principal aims of this study is to test numerically the connection between this stability weight and the statistical probability of the UPO. We can use all these facts to compute the averages of thermodynamic quantities. What needs to be done then is to consider the dynamics for UPOs of finite n, and then extrapolate the results to the $n \to \infty$ limit. If B is a function of phase only, then the average value of B over the chaotic set can be written as

$$\langle B \rangle = \lim_{n \to \infty} \frac{\sum_{i \in P_n} \Lambda_i^{-1} \int_0^{\tau_i} B(s)\, ds}{\sum_{i \in P_n} \tau_i \Lambda_i^{-1}} \tag{8}$$

where τ_i is the period for the ith UPO, and the integral is over the ith UPO. Vance[7] has used this *periodic orbit expansion* (POE) for the Lorentz gas in an external field to obtain the diffusion coefficient as the ratio of the mass current to the external field. Vance also derived the equilibrium periodic orbit expansion for the diffusion coefficient in the absence of a field, which takes the form

$$D = \lim_{n \to \infty} \frac{1}{2d} \frac{\sum_{i \in P_n} (\Delta \mathbf{r}_i)^2 \Lambda_i^{-1}}{\sum_{i \in P_n} \tau_i \Lambda_i^{-1}} \tag{9}$$

where $(\Delta \mathbf{r}_i)^2$ is the square of the displacement of the wandering particle along one transit of the ith UPO and d is the dimensionality of the Lorentz gas (here $d = 2$). Formulas related to Eq. (8) have been derived in different ways.[7,8,12]

To illustrate the ideas involved in the periodic orbit expansion, we present a heuristic derivation of the formulas which are used to compute averages of phase and dynamic variables in such a context. If we consider the probability measure supported over the set of periodic orbits with n collisions, ρ_n say, then this assigns the same *mass* (or probability) to each point on the same cycle, and it is reasonable to assume that such a quantity is proportional to the stability of the orbit. The argument is that the more unstable the orbit, the less likely it is to be approached in phase space compared with those orbits which are less unstable (dynamically, a phase

space trajectory visits regions of higher natural measure more often). Thus, we may adopt a measure which is proportional to the inverse of the Lyapunov number of the UPO when evaluated over a segment of that UPO, and that vanishes outside the set of points covered by the UPO. Note that we can parametrize every point on a given orbit either by its distance in curvilinear coordinates from a fixed origin on the orbit or by the time that it takes to travel along the orbit from that origin (since the speed of our particles is equal to one). In our work, for convenience, we use the time variable. Then, the measure of a segment of the jth UPO with n collisions is $d\rho_{j\in P_n}(t) = C\Lambda_j^{-1}\, dt$, where Λ_i^{-1} is the inverse Lyapunov number, and C is a normalization constant independent of i. The contribution to the average of an arbitrary phase variable B from that periodic orbit can be written as

$$\langle B\rangle_{j\in P_n} = \int B(s)\, d\rho_{j\in P_n}(t) = C\Lambda_j^{-1} \int_0^{\tau_j} B(s(t))\, dt \tag{10}$$

In turn, the measure ρ_n is given by the sum of pieces like $\rho_{j\in P_n}$ for all the j in P_n, and the average of B over all prime cycles with n collisions takes the form

$$\langle B\rangle_n = \frac{\sum_{j\in P_n} \Lambda_j^{-1} \int_0^{\tau_j} B(t)\, dt}{\sum_{j\in P_n} \tau_j \Lambda_j^{-1}} \tag{11}$$

where the normalization constant C is easily found by taking $B = 1$ (probability conservation). Now, recalling that the measure on the chaotic attractor is approximated by periodic cycles of larger and larger period, we see that it is enough to take the limit $n \to \infty$ to get Eq. (8).

It appears that Eq. (8) represents both a time and space average of the variable B, but this is simply one interpretation of the measure. If, after constructing the measure, we ignore the periodic points or UPOs that gave rise to it, then the measure can be viewed as an approximation to the natural measure and can be used as such in pure phase space averages. If, however, we ask for the probability of observing a particular cycle or UPO, i say, among those with the same number of collisions, then that is given by

$$\rho_i = \frac{\tau_i \Lambda_i^{-1}}{\sum_{j\in P_n} \tau_j \Lambda_j^{-1}} \tag{12}$$

where the sum is intended over prime UPOs.

To calculate the potential part of the pressure p^ϕ for the system, we rewrite Eq. (7) as a sum over collisions, so that

$$\langle p^\phi\rangle V = -\lim_{t\to\infty} \frac{1}{t} \sum_{\text{collisions}} p_{12}\cdot r_{12} = -\lim_{t\to\infty} \frac{1}{t} \sum_{\text{collisions}} p\cdot r \tag{13}$$

and its periodic orbit expansion can be written as

$$\langle p^{\phi} V \rangle = \lim_{n \to \infty} \frac{\sum_{i \in P_n} \sum_{\text{collisions}} |p \cdot r| \Lambda_i^{-1}}{\sum_{i \in P_n} \tau_i \Lambda_i^{-1}} \tag{14}$$

where p is the relative momentum immediately before collision and σ is the diameter of a hard disk (or the radius of the scatterer).

To explore the utility of the periodic orbit expansions, we calculate three different properties: the potential contribution to the hydrostatic pressure, a standard thermodynamic property which can be calculated very accurately as a time average; the diffusion coefficient; and the average Lyapunov exponent. The average Lyapunov exponent $\langle \lambda \rangle$ is the largest exponent for the whole system, rather than the value for a particular UPO. That is,

$$\langle \lambda \rangle = \lim_{n \to \infty} \frac{\sum_{i \in P_n} \lambda_i \tau_i \Lambda_i^{-1}}{\sum_{i \in P_n} \tau_i \Lambda_i^{-1}} \tag{15}$$

4. SYMBOLIC DYNAMICS FOR THE LORENTZ GAS

In the elementary cell (EC) we can generate a symbol sequence by assigning a symbol to each section of trajectory between collisions. The symbol that is assigned depends upon the vector separation between the centers of the scatterers involved in the initial and final collisions for that segment of trajectory. For a UPO the symbol sequence uniquely defines the orbit, so that the terms in the periodic orbit expansion can be enumerated by determining all possible symbol sequences composed of a fixed number of symbols. One must then *prune* that list of symbol sequences by removing those orbits that pass through scatterers and are hence not physically realizable. We will use symbolic dynamics to distinguish different UPOs in our simulations and also to determine the degeneracy of a particular UPO. By degeneracy we mean the number of different physical orbits which are related by discrete symmetries and make the same contribution to the averages. This is directly related to the degree of symmetry of the orbit within the triangular lattice. For a fuller discussion of the exploitation of symmetry see ref. 20.

Figure 4 shows the lattice of scatterers with the 12 possible flights labeled. Due to the finite horizon, these are the only flights that are possible. In the figure even numbers correspond to short flights between nearest neighbors and odd numbers to the long flights between second nearest neighbors. We now give a complete description of the admissible UPOs with less than seven collisions for a spacing of $w = 0.3$.

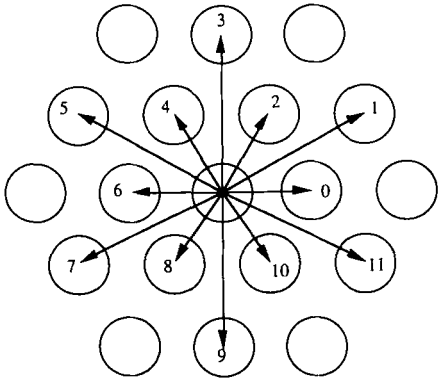

Fig. 4. The symbols associated with each of the possible flights between scatterers.

There are four types of length-two UPOs (i.e., UPOs with two collisions): the short flight (S) between nearest neighbor scatterers; the long flight (L) between second nearest neighbors; the tick-shaped orbit (T), consisting of a long flight and a short flight; and the V-shaped orbit (V) of two long flights (see Fig. 5). It is easy to see that the S UPO can have the following symbol sequences:

$$\text{S} \qquad (0\,6),\ (2\,8),\ (4\,10),\ (6\,0),\ (8\,2),\ (10\,4) \tag{16}$$

Of these six orbits, only three are distinct. The orbits 0–6 and 6–0 are the same orbit with different beginning points. We can also think of the orbits 6–0 and 0–6 being related by plus or minus the lattice vector in the x direc-

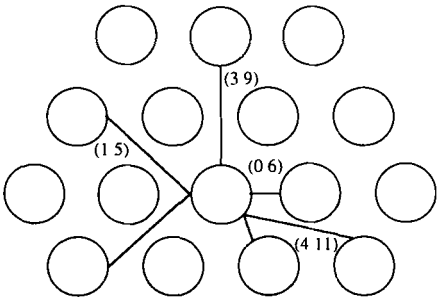

Fig. 5. Examples of length-2 UPOs. (0 6) is the short flight orbit; (3 9) is the long flight orbit; (4 11) is the tick orbit; and (1 5) is the V orbit.

tion. The case of the long flight orbit L is similar. The possible sequences are

$$\text{L} \quad (1\,7),\ (3\,9),\ (5\,11),\ (7\,1),\ (9\,3),\ (11\,5) \tag{17}$$

Again only three of these symbol sequences are distinct. The tick-shaped UPO consists of a short flight followed by a long flight and in this case there are 12 distinct symbol squences:

$$\begin{aligned} \text{T} \quad & (2\,7),\ (4\,9),\ (6\,11),\ (8\,1),\ (10\,3),\ (0\,5) \\ & (0\,7),\ (2\,9),\ (4\,11),\ (6\,1),\ (8\,3),\ (10\,5) \end{aligned} \tag{18}$$

We can think of the first two orbits (S and L) as being symmetric about their center (or under reflection), whereas T is asymmetric. The last orbit V is again symmetric about its center and there are six possibilities:

$$\text{V} \quad (7\,11),\ (9\,1),\ (11\,3),\ (1\,5),\ (3\,7),\ (5\,9) \tag{19}$$

All of these six possibilities are distinct.

The total number of length-two orbits is 24, which is made up of three S, twelve T, three L, and six V orbits. One way of thinking about these orbits is in terms of short and long flights. Short flights are between nearest neighbors and long flights are between second nearest neighbors. The UPOs S, L, and V are made of two similar orbits, either both short or both long flights; whereas the T orbit consists of one short and one long flight. Clearly, it is possible for UPOs composed of two similar flights to have more symmetry than UPOs composed of different flights. This symmetry determines what we call the degeneracy of the orbit—that is, the number of different symbol string representations for the orbit. For the T orbit we have seen that there are 12 different symbol strings which all have the same contribution to an average property. These 12 different strings can be obtained from a single symbol string by rotating that orbit around the center of the EC, or by reflecting it about the horizontal direction, or by reversing the direction of the motion. To reduce the number of orbits we need to consider, we define the *fundamental representation* (or fundamental symbol string) for a group of symmetry-related orbits and its degeneracy. From the symbolic representation for an orbit we obtain an integer by interpreting the symbol string as a base-12 number. That is, to the symbol $s_n,\ldots, s_1$ we assign an integer I_n deined by

$$I_n = \sum_{i=1}^{n} 12^{i-1} s_i$$

The fundamental representation of a group of symmetry-related orbits is

Table II. Periodic Orbits of Length 2

Orbit	Degeneracy	$\lambda\tau$	Symbol
S	3	1.51286399	(0 6)
T	12	3.15831208	(0 5)
L	3	3.51394510	(1 7)
V	6	4.65944481	(1 5)

that symbol sequence that has the smallest base-12 integer I_n, and the degeneracy is the number of different symmetry-related orbits. For example, for the T orbit the fundamental symbol string is (0 5), which has degeneracy 12. Given the fundamental symbol sequence, all the symbol sequences for the group can be obtained by applying one or more of the symmetry operations: rotation, reflection, and time reversal. Each of these symmetry operations has a simple meaning when we consider its action upon a symbol string. For example, the six rotations can be obtained by adding either 0, or 2, or 4, or 6, or 8, or 10 modulo 12, to each symbol in the symbol sequence. The reflection in the x axis is obtained by taking the negative mod 12 of each symbol. Time reversal consists of reversing the order of the symbol string and adding 6 mod 12 to each symbol. Table II is the table of orbits with two collisions (length 2) at $w = 0.3$, giving both the fundamental symbol sequence and the degeneracy. The Lyapunov numbers are given by $\exp(\lambda\tau)$, where λ is the Lyapunov exponent and τ the period.

We note that all the orbits from the groups S, L, T, and V are periodic in the EC. But the S and L orbits actually are periodic in the whole phase space, so that $\Delta r(t)^2$ is bounded for all t, while the T and V orbits are not closed and $\Delta r(t)^2 \sim t^2$ at large t.

All length-three UPOs can be considered as variations upon length-two UPOs. The first is the small triangle T made up of three short flights (which we can think of as adding an extra short flight to S). The symbol sequences for this orbit are (2 6 10), (2 10 6), (0 4 8), (0 8 4). The variation

Table III. Periodic Orbits of Length 3

Orbit	Degeneracy	$\lambda\tau$	Symbol
S′	4	3.27128792	(0 4 8)
L′	12	6.23520184	(0 2 7)
T′	24	6.31880379	(0 2 6)
V′	24	8.30080318	(0 2 5)

of the long-flight UPO L changes one long flight into a glancing collision and hence two short flights. For example, (1 7) becomes (0 2 7). The variation on the tick orbit T replaces the long flight with a glancing collision of two short flights, so that (0 5) becomes (0 4 6), which in turn becomes (0 2 6) under time reversal and rotation. This orbit consists of three short flights but is not closed. The variation on the V orbit replaces one of the long flights with a glancing collision. For example, (1 5) becomes (0 2 5). The resulting orbit is open and consists of two short and one long flight. Table III is the table for the orbits with three collisions.

5. THE RUELLE ζ-FUNCTION FORMALISM

A number of recent works (see, e.g., refs. 5, 8, 11, 12, and 17 and references therein) have discussed the Ruelle ζ-function formalism[18] and its adaption to compute average quantities of physical interest from many kinds of dynamical systems. In this section we outline that development. In statistical mechanics it is important to develop a method of calculating the averages of arbitrary phase variables. To do this we consider the combined time and space average of the phase variable B[12,8] and exploit the solid framework of probability theory, introducing generating functions whose moments provide the averages we need. We outline the argument below for discrete-time systems, in this case a mapping of the unit interval. To begin we define the function $Q(\beta)$ where

$$Q(\beta) = \lim_{n \to \infty} \frac{1}{n} \ln \langle \exp[\beta B^n] \rangle = \lim_{n \to \infty} \frac{1}{n} \ln \int_0^1 dx\, \rho_n(x) \exp[\beta B^n(x)] \quad (20)$$

where $B^n(x)$ is the sum of the values of B along a length-n orbit beginning at the point x. To obtain the usual form for the average we differentiate with respect to β and then set $\beta = 0$;

$$\left. \frac{dQ}{d\beta} \right|_{\beta = 0} = \lim_{n \to \infty} \frac{1}{n} \int_0^1 dx\, \rho_n(x) \sum_{i=1}^{n} B(x_i(x))$$

This is the ensemble average of the discrete-time average of B. We choose initial values of x according to their probabilities $\rho_n(x)$ and then generate the discrete-time average beginning at the point x. Consider the formal sum over periods of all lengths

$$\Omega(z) = \sum_{n=1}^{\infty} z^n \langle \exp[\beta B^n] \rangle = \sum_{n=1}^{\infty} z^n \int_0^1 dx\, \rho_n(x) \exp[\beta B^n] \quad (21)$$

We remark that as $n \to \infty$ the sum $B_j^n = \sum_{i=0}^{n-1} B(x_{ij}) \to n \langle B \rangle$ (where $\langle B \rangle$

is the standard time average of B), so that the generating function behaves as

$$\Omega(z) \sim \sum_{n=1}^{\infty} z^n \exp(\beta n \langle B \rangle) = \frac{z \exp(\beta \langle B \rangle)}{1 - z \exp(\beta \langle B \rangle)}$$

This implies that the divergence of the generating function $\Omega(z)$ occurs when $\langle B \rangle = -(1/\beta) \ln z$. Substituting the limiting form of $\langle B \rangle$ into Eq. (20) for $Q(\beta)$, we find that

$$Q(\beta) \sim \lim_{n \to \infty} \frac{1}{n} \ln \langle \exp[n\beta \langle B \rangle] \rangle = \beta \langle B \rangle$$

and hence $\Omega(z)$ diverges when $-\ln z = Q(\beta)$. Taking Eq. (21) and substituting the stability weights for the periodic orbits gives

$$\Omega(z) = \sum_{n=1}^{\infty} z^n \sum_j \Lambda_j^{-1} \exp[\beta B_j^n] \tag{22}$$

where we have labeled periodic cycles with the index j. The sum over j contains each prime cycle beginning from each of its possible starting points and multiple traversals of all prime cycles, so we rewrite this as a sum over prime cycles

$$\Omega(z) = \sum_p n_p \sum_{r=1}^{\infty} \left(\frac{z^{n_p} e^{\beta B_p}}{|\Lambda_p|} \right)^r = \sum_p \frac{n_p z^{n_p} e^{\beta B_p} |\Lambda_p^{-1}|}{1 - n_p z^{n_p} e^{\beta B_p} |\Lambda_p^{-1}|} \tag{23}$$

where $B_p = \sum_{i=0}^{n_p - 1} B(x_i)$ is the sum of the values of B around the prime UPO. If we define

$$t_p = \frac{z^{n_p} e^{\beta B_p}}{|\Lambda_p|} \tag{24}$$

then we have that

$$\Omega(z) = \sum_p \frac{n_p t_p}{1 - t_p} \tag{25}$$

Defining the Ruelle ζ function as

$$\frac{1}{\zeta(\beta, z)} = \prod_p (1 - t_p) = \prod_p (1 - z^{n_p} e^{\beta B_p} |\Lambda_p^{-1}|) \tag{26}$$

then taking the logarithm and differentiating with respect to z, we can show that the generating function Ω is related to the Ruelle ζ-function by

$$\Omega(\beta, z) = -z \frac{d}{dz} \ln\left(\frac{1}{\zeta(\beta, z)}\right) \tag{27}$$

In Eq. (21) we have shown that finding the average of B *corresponds* to finding the value of z for which $\Omega(z)$ diverges. This occurs when

$$-\ln z = \beta \langle B \rangle = Q(\beta) \tag{28}$$

which suggests a change in the definition of t_p replacing $-\ln z$ by a new variable s, so that

$$t_p = \frac{e^{\beta B_p - n_p s}}{|\Lambda_p|} \tag{29}$$

Then $Q(\beta)$ can be found from the solution of

$$\frac{1}{\zeta(\beta, Q(\beta))} = \prod_p (1 - t_p) = 0 \tag{30}$$

As an example of the implementation of the ζ-function formalism to generate what we will refer to as *cycle expansions*, we consider the calculation of the average Lyapunov exponent and diffusion coefficient. We have

$$\langle \lambda \rangle = \lim_{t \to \infty} \frac{1}{t} \langle \ln \Lambda'(x) \rangle$$

so the phase variable to consider is $\ln \Lambda = \lambda \tau$, and the weight function for the Ruelle dynamical ζ-function is

$$t_p = \frac{e^{\beta \ln \Lambda_p - s\tau_p}}{|\Lambda_p|}$$

The ζ-function-based cycle expansion for the average Lyapunov exponent can be written as[8]

$$\langle \lambda \rangle = \frac{\sum_{p_1 \cdots p_k} (-1)^k (\ln \Lambda_{p_1} + \cdots + \ln \Lambda_{p_k})/|\Lambda_{p_1} \cdots \Lambda_{p_k}|}{\sum_{p_1 \cdots p_k} (-1)^k (\tau_{p_1} + \cdots + \tau_{p_k})/|\Lambda_{p_1} \cdots \Lambda_{p_k}|} \tag{31}$$

where $p_1 \cdots p_k$ is the symbol string for the prime UPO. An arbitrary symbol string may be decomposable into smaller substrings where all the

substrings are themselves prime UPOs. In that case k is the number of substrings. The cycle expansion formula for the diffusion coefficient is[8]

$$D=\frac{1}{2d}\frac{\sum_{p_1\cdots p_k}(-1)^k(n_{p_1}^2+\cdots+n_{p_k}^2)/|\Lambda_{p_1}\cdots\Lambda_{p_k}|}{\sum_{p_1\cdots p_k}(-1)^k(\tau_{p_1}+\cdots+\tau_{p_k})/|\Lambda_{p_1}\cdots\Lambda_{p_k}|} \tag{32}$$

where $d=2$ for the two-dimensional Lorentz gas and $\hat{n}_{p_i}$ is the displacement obtained from the UPO with symbol string p_i. Equations (31) and (32) are the cycle expansion formulas for $\langle\lambda\rangle$ and D.

From Eq. (21), putting $\beta=0$, it can be shown that $\Omega(z)=z/(1-z)$. Using Eq. (27), we find that $\zeta(0,z)=1/(1-z)$, so that the first zero of the ζ function is at $z=1$. Substituting this into Eq. (26) gives

$$1-\sum_{p_1\cdots p_k}(-1)^k/|\Lambda_{p_1}\cdots\Lambda_{p_k}|=0 \tag{33}$$

This last expression can be used to check the numerical accuracy of the cycle expansion truncated after a fixed number of collisions. This is a very important check of the quality and numerical consistency of the evaluation of cycle expansions.[19]

To evaluate the cycle expansions in Eqs. (31) and (32), which are written as sums over all possible symbol strings, we need to be able to both identify all allowed symbol strings and all subdivisions of that symbol string where each substring is also an allowed UPO. However, in practice we find that it is easier to construct all symbol strings of a fixed length n by finding all prime UPOs of that length and all products of smaller UPOs whose product string is of length n. For example, when we deal with orbits with four or more collisions, we find that combinations of orbits of smaller period UPOs (e.g., the product of two length-two UPOs), are product strings in the cycle expansion. The motivation for ordering the cycle expansions in this way is that, for example, the product string (0 5)(0 6) is a reasonable approximation to the string (0 5 0 6) and each of these produces a term in the cycle expansion with a different sign. Thus the cycle expansion contains $t_{0506}-t_{05}t_{06}$, which is approximately zero. In the Ruelle ζ-function cycle expansions these types of terms can be conveniently grouped together to form so-called *curvature corrections*.[12] Such *curvature corrections* can be simple terms composed of a prime string t_{0506} minus a single *shadowing approximant* $t_{05}t_{06}$ such as in the previous example, or they can be more complicated. The expansion of the Ruelle ζ-function can then be written as

$$\frac{1}{\zeta}=\prod_p(1-t_p)=1-\sum_f t_f-\sum_n c_n \tag{34}$$

where c_n are the curvature corrections and t_f are fundamental cycles with no shorter approximants. The motivation behind this approach is the claim that the sum of curvature corrections quickly converges to zero, and therefore this reordering of the expansion leads to a better approximation to the ζ-function. Unfortunately, the following analysis shows that this is not the case for the Lorentz gas.

In Table IV we list the orbits of length 4 for $w = 0.3$, with their fundamental symbol sequences and associated approximants. There are several points to note about the shadowing approximants. First, not all prime symbol strings have shadowing approximants, and second it is possible for there to be more than one approximant for a particular string. If the prime string has a single approximant, then a simple *curvature* term $t_{AB} - t_A t_B$ can be formed whose value is close to zero. From Table IV this can be done for four of the prime symbol strings. However, the first of these (0 4 10 6) has a degeneracy of six, while the product string (0 6)(0 6) has a degeneracy of nine. This mismatch in degeneracy destroys the cancellation property. Further, there are many prime symbol strings without shadowing approximants, and also many more product strings whose prime string is pruned (that is, not allowed). All of these observations, together with the fact that decreasing the spacing between the scatterers alters the number of matching terms even more, suggest that reordering the periodic orbit expansion to obtain cycle expansions like Eq. (34) will not

Table IV. Periodic Orbits of Length 4

Degeneracy	$\lambda\tau$	Symbol	Approximant
6	4.34599781	(0 4 10 6)	(0 6)(0 6)
12	4.61036587	(0 5 0 6)	(0 5)(0 6)
6	5.57779312	(0 4 0 8)	Prime
6	5.58333111	(0 5 0 7)	(0 5)(0 5)
12	6.21474981	(0 5 1 6)	(0 5)(0 5) and (0 6)(1 5)
12	6.31094980	(0 4 0 7)	Prime
12	6.42766714	(0 2 4 8)	Prime
12	7.08779097	(0 3 0 8)	Prime
12	7.47488117	(0 4 0 6)	Prime
12	7.78748178	(0 3 0 7)	Prime
12	7.81867790	(0 5 1 5)	(0 5)(1 5)
6	8.19202900	(0 2 6 8)	Prime
6	8.58509731	(0 3 0 9)	Prime
6	9.44087410	(0 2 8 6)	Prime
12	10.1162662	(0 4 0 5)	Prime
12	11.3982677	(0 2 4 6)	Prime
12	12.0706491	(0 2 6 4)	Prime

Table V. Products of Length-2 Orbits

	S	T	L	V
S	3	36	9	18
T		66	36	72
L			3	18
V				15

lead to improved convergence. To make these arugments more concrete, let us see what happens for the case where the pruning of orbits is least: $w = 0.3$.

At length 4, the expansion of the dynamical ζ-function produces a great number of products of length-2 UPOs. Consider the 24 length-2 symbol strings. From these we can generate $24 \times (24-1)/2 = 276$ possible product strings compared with 168 prime strings. The degeneracy of the product string can be found from the degeneracies of its composite strings. The possible products and their degeneracies are summarized in Table V. The degeneracies of length-2 UPOs lead to the generation of large numbers of product terms, many of which are not needed as terms in length-4 curvature corrections. The number of the matching terms actually used in curvature corrections of the form $t_{AB} - t_A t_B$ is listed in Table VI. The great excess of product strings means that the curvature corrections are not balanced, which has a negative effect on the convergence properties of the cycle expansion. Indeed, to have good convergence we would like to have cancellation of terms by grouping them as in $t_{AB} - t_A t_B$.[12] This feature appears to be lost because the number of $t_A t_B$ terms greatly exceeds the number of t_{AB} terms. (Indeed this pairwise matching is not even possible for a complete binary dynamics.[12])

At length 5 there are 1536 possible product strings, and only 516 prime strings. At length 6 we have triple products of length-2 UPOs (2024) as well as simple products of both length 2 and 4 (4464), and two length-3

Table VI. Products of Length-2 Orbits Needed for Matched Curvature Corrections

	S	T	L	V
S	6	12	0	12
T		18	0	12
L			0	0
V				0

UPOs (2016). Altogether, there are 1262 prime strings with a minus sign, 6480 products with a plus sign, and 2024 products with a minus sign. Clearly there can be very little cancellation when this is rearranged into curvature correction terms, and the problem worsens at smaller values of w where the pruning of UPOs is even stronger.

6. NUMERICAL SCHEME

To evaluate the periodic orbit expansions we follow a similar numerical scheme to that proposed by Vance.[7] From a chaotic trajectory of typically 10^{10} collisions we scan the collision sequence at the collision time for approximate recurrences of a phase point (ϕ_i, θ_i). If $\|(\phi_{i+j}, \theta_{i+j}) - (\phi_i, \theta_i)\| < 10^{-3}$, then we save (ϕ_i, θ_i) as the initial condition for a UPO of length j (UPO with j collisions). Each possible UPO initial condition is then refined using a Newton–Raphson iteration scheme and its largest Lyapunov number Λ_i calculated by following a tangent vector of size $0.5*10^{-11}$ to 10^{-10} around the UPO ten times. The Lyapunov number is calculated from the final transit around the UPO, with earlier transits allowing the tangent vector time to seek out the fastest growing direction in phase space. This scheme allowed the Lyapunov exponent to be calculated to about six significant digits for UPOs of 2–12 collisions. It is clear that the instability of a UPO measured by the Lyapunov number affects the convergence of the Newton–Raphson refinement scheme. The average separation of a trajectory from an exact UPO is given by $l(t) = l(0)\,\Lambda_i$. If, for example, the Lyapunov number is $\Lambda_i = \exp(\lambda_i \tau_i) = \exp(13.8)$ and the initial phase point (ϕ_i, θ_i) is within 10^{-10} of the exact UPO, then on average, after one cycle of the approximate UPO the separation has grown to 10^{-4}. In practice this places a natural limit upon the maximum observable Lyapunov number, and our method of sampling UPOs ensures that we sample the most probable ones thoroughly, but it is possible that unpruned UPOs with relatively high Lyapunov numbers may be neglected.

Gaspard and Baras[5] have shown that it is possible to calculate the largest Lyapunov exponent for a section of a trajectory analytically using the Sinai formula for the curvature of an unstable front. Indeed, for a periodic orbit the calculation of the largest exponent is obtained by solving a quadratic equation.[17] On the other hand, Cvitanovic *et al.* calculate the Lyapunov numbers by finding the eigenvalues of the stability matrix for the time evolution.[19] Our numerical results for the Lyapunov numbers are in excellent agreement with the analytic results obtained from both of these methods. We have also calculated the Lyapunov exponents analytically using the Sinai formula for all UPOs and our numerical results are in excellent agreement with the latter. Note that the numbers in our tables are

from our numerical scheme, which is a standard method also applicable when analytic formulas are not available. Moreover, even the analytic formula needs trajectory information that can only be obtained numerically.

In the calculations of the periodic orbit expansion, using Eq. (9), for example, we exploit the fact that the set of prime orbits contains d_i copies of the same contribution, where d_i is the degeneracy of a particular UPO, by reducing the summation to one over fundamental symbol strings. Then Eq. (9) becomes

$$D = \lim_{n \to \infty} \frac{1}{2d} \frac{\sum_{i \in F_n} d_i (\Delta r_i)^2 \Lambda_i^{-1}}{\sum_{i \in F_n} d_i \tau_i \Lambda_i^{-1}} \tag{35}$$

where F_n is the set of fundamental symbol strings of length n. The degeneracy and the set of fundamental symbol strings are used in a similar way to reduce the numerical complexity of the cycle expansions in Eqs. (31) and (32) as well.

7. RESULTS AND DISCUSSION

In Fig. 6 we plot the probability of a UPO (as measured by its frequency of occurrence in the simulation) versus the stability weight ρ_j associated with it in the periodic orbit expansion [as given by Eq. (12)] for

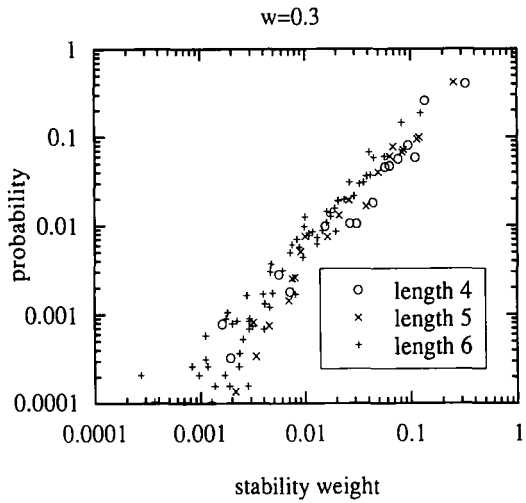

Fig. 6. The probability of finding a particular unstable periodic orbit (UPO) versus the stability weight associated with it in the periodic orbit expansion, for UPOs of length 4, 5, and 6 at $w = 0.3$. The linear relationship illustrates that the probability and the stability weight are strongly correlated.

UPOs of length 4, 5, and 6 for a disk separation $w = 0.3$. For each of the values of n, we ran a simulation which identified several tens of thousand UPOs, from which the frequency of occurrence was determined. It is interesting to note that the relation between the ρ_j and the corresponding frequencies appears to be the same at all lengths. Also, the spreading of points at low values of the frequencies is most likely to be attributed to the poor statistics available at that level. Indeed, some of the points correspond to UPOs which were observed only once in the simulation. If the stability weights are simply related to the statistical probability of observing the UPO, then we would observe a linear proportionality. This is indeed observed for lengths of 4, 5, and 6 for $w = 0.3$, and the line appears to be relatively independent of the length. This means that Eq. (12) is not only a good approximation to the relative probabilities of UPOs of a fixed length, but it may be used to compare the probabilities of individual UPOs of different lengths, even for UPOs as short as length 4. This is a vindication of the arguments used to derive the dynamical weights used in the periodic orbit expansion.

In the remainder of this section we present and compare the results obtained using the periodic orbit expansion [Eq. (8)] and the cycle expansion [Eqs. (31) and (32)] at a variety of different interdisk spacings. In both approaches the convergence can be accelerated. This point is important as we test the efficiency and accuracy of the methods, and the ability of an acceleration scheme may play a fundamental role[8,20] in this comparison. For the periodic orbit expansions, a pronounced odd–even effect is often observed and this can be removed using the Shanks transformation.[21] If the nth term in a sequence takes the form $A_n = A + \alpha q^n$, with $|q| < 1$, so that $A_n \to A$ as $n \to \infty$, then the sequence

$$C_n = \frac{A_{n+1}A_{n-1} - A_n^2}{A_{n+1} + A_{n-1} - 2A_n} \tag{36}$$

may be a more rapidly convergent approximation. If so, then this increase in convergence comes at almost no extra computational cost. However, there are circumstances where the Shanks transformation will not improve the convergence, so some caution must be exercised. To improve the convergence of the cycle expansions it is very useful to exploit the symmetry of the system in the calculation of the ζ-function. This is done by reducing the dynamics to the *fundamental domain* (FD) which is 1/12 of the EC, and in ref. 8 this has been carried out for $w = 0.3$. The difficulty with this approach is that so far it has not been possible to obtain an explicit formula for the diffusion coefficient using the fundamental domain [the analog of Eq. (32)] and this severely limits the approach.

Table VII. Periodic Orbit Expansion for $w = 0.3$

n	# cycles	$p^{\phi}V$	D	λ	$\sum \tau_i \Lambda_i^{-1}$
2	24	0.4813	0.3754	1.3304	2.3971
3	64	0.5194	0.1624	1.9408	0.4978
4	168	0.4542	0.3800	1.5180	1.1758
5	516	0.5108	0.1979	1.8012	0.6662
6	1262	0.5203	0.3109	1.6445	0.8783
7	4200	0.5344	0.2418	1.7765	0.7056
8	14652	0.5407	0.2658	1.7166	0.8098
9	51252	0.5404	0.2400	1.7582	0.7304
10	165150	0.5467	0.2501	1.7421	0.7569
Direct	—	0.5457	0.2492(3)	1.7565	—

In Tables VII–IX we present the results obtained for a spacing of $w = 0.3$. We compare our periodic orbit expansion results with those obtained in Section 2. We refer to the estimates of Section 2 as the *direct* results. The numerical accuracy of the pressure calculation is quite good, $\sim 1\%$; however, the value of D is a little more difficult to obtain, as all the closed orbits contribute zero, and those orbits that contribute most are often the most unstable. The result obtained at length 10 is about 2% low, whereas the results at lengths 8 and 9 bracket the correct result. The value of the Lyapunov exponent is within 0.5% of the best available estimate of 1.7565.[8]

We can also reprocess the data in Table VII using the Shanks transformation, to improve the convergence of sequences with a strongly oscillating behavior. The results are reported in Table VIII. The value for the pressure is a little lower with the same error, $\sim 1\%$, but the diffusion coefficient is within 2.5%.

Table VIII. Shanks Transformation for $w = 0.3$

n	$p^{\phi}V$	D	λ	$\sum \tau_i \Lambda_i^{-1}$
3	0.4953	0.2700	1.6910	0.9974
4	0.4845	0.2809	1.6876	0.8849
5	0.5221	0.2677	1.7003	0.8159
6	0.4918	0.2680	1.7162	0.7831
7	0.5458	0.2596	1.7353	0.7706
8	0.5404	0.2534	1.7411	0.7647
9	0.5407	0.2473	1.7466	0.7503
Direct	0.5457	0.2492(3)	1.7565	—

Table IX. Cycle Expansion for $w=0,3$

n	# cycles	$p^{\phi}V$	D	λ	$\zeta(0,0)^{-1}$
2	24	0.4813	0.3754	1.3304	−0.3170
3	64	0.4878	0.3388	1.4353	−0.5415
4	168	0.5512	0.2548	1.9029	−0.0976
5	516	0.6093	0.1772	2.2986	0.01964
6	1262	0.5770	0.1842	1.8701	0.0300
7	4200	0.5842	0.2255	1.7896	0.0264
8	14652	0.5522	0.2684	1.7021	−0.0015
9	51252	0.5442	0.2560	1.6905	−0.0055
10	165150	0.5591	0.2384	1.7408	0.0071
Direct	—	0.5457	0.2492(3)	1.7565	—

The results for the cycle expansion at $w=0.3$ are similar to those for the periodic orbit expansion. The pressure is within 4% at length 10, but considerably better at length 9. The diffusion coefficient is bracketed by the results at lengths 9 and 10, but the result at length 10 is about 8% too low. The Lyapunov exponent result at length 10 is excellent, whereas at lengths 8 and 9 it is relatively poor. The last column gives $\zeta(0,0)^{-1}$, which must be rigorously zero. This is probably the best consistency check on the numerical adequacy of the sampling of cycles. Our results suggest that at lengths 8 and 9 we have a very good sampling of the allowed cycles, but at length 10 our sampling is not quite as good. It is most important to realize that the same set of UPOs is used in both the periodic orbit expansion and the cycle expansion; the difference is only in the expansion formula.

In the two approaches that we have considered there are methods to improve convergence. For the POE we can apply the Shanks transformation to improve convergence if the raw results are oscillatory, and for the cycle expansions we can reformulate them in the fundamental domain (exploiting cycle symmetry). In Table VII we compare these two different approaches, the Shanks transformation applied to POE and the cycle expansions in the EC, with those in the fundamental domain. This comparison is made in Figs. 7 and 8 for the Lyapunov exponent at $w=0.3$. Note that the fundamental domain results are those taken directly from ref. 8. In Fig. 7 we see that both the Shanks transformation for the POE, and the fundamental domain for the cycle expansion, greatly improve the reliability of the two methods, and the final accuracies are essentially equivalent. When both methods can be applied they give results of the same accuracy, but the Shanks transformation is considerably simpler to implement.

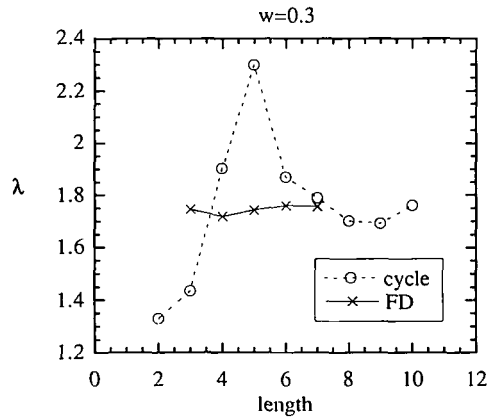

Fig. 7. The cycle expansion results for the average Lyapunov exponent at $w = 0.3$. The circles are for the results for the elementary cell; the crosses are the results for the fundamental domain taken from ref. 8.

Our results for the state point $w = 0.236$ are listed in Tables X and XI. At this smaller value of the spacing there is more pruning of orbits, although the numbers of length 2 and 3 have not changed. At length 4 the number of fundamental strings has decreased from 17 to 12. This means that the number of UPOs has decreased from 168 to 108.

Vance[7] has used the periodic orbit expansion to calculate the diffusion coefficient at this state point. His calculations are somewhat different

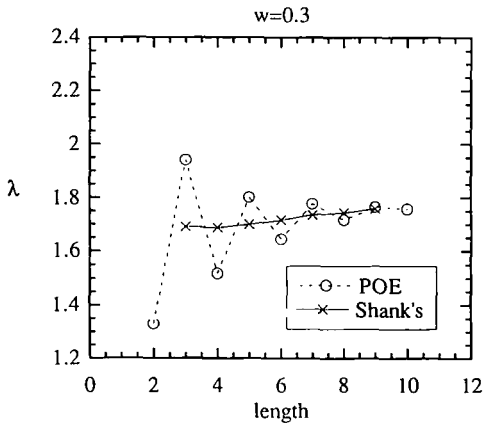

Fig. 8. The periodic orbit expansion results for the average Lyapunov exponent at $w = 0.3$. The circles are the periodic orbit expansion (POE) using Eq. (9); the crosses are obtained from the Shanks transformation of the same results.

Table X. Periodic Orbit Expansion for $w = 0.236$

n	# cycles	$p^{\phi}V$	D	λ	$\sum \tau_j A_j^{-1}$
2	24	0.5430	0.3769	1.4053	2.3656
3	64	0.6457	0.0901	2.0757	0.4292
4	108	0.5411	0.3146	1.6618	1.0484
5	252	0.6326	0.1269	1.9803	0.5260
6	716	0.6164	0.2477	1.7699	0.8310
7	2184	0.6332	0.1771	1.9733	0.5733
8	5952	0.6511	0.2228	1.8926	0.7027
9	19196	0.6482	0.1885	1.9607	0.6010
10	51072	0.6628	0.2084	1.9329	0.6352
Direct	—	0.665(1)	0.1970(10)	—	—

from those reported here, as he considers the Lorentz gas subjected to an applied external field and calculates the induced current. For a field $E = 0.01p^2/m\sigma$ he finds a diffusion coefficient of 0.100, which is in agreement with the extrapolated results of ref. 4. Our results for POE are presented in Table X. The result for the pressure is excellent (within 1%), while the diffusion coefficient is bracketed by the results at lengths 9 and 10. Length 9 is 5% too low, while length 10 is 5% too high. The Shanks estimate is much better, being about 2% too high.

In the cycle expansion results for $w = 0.236$ we observe some seemingly spurious negative numbers for the average properties at lengths of 4, 5, and 6. This is the direct result of the very strong pruning at this state point. There are the same number of length-2 and-3 UPOs as we have for $w = 0.3$ hence the same number of product strings of lengths 4, 5, and 6. However, the number of prime length-4 UPOs has fallen from 168 (at $w = 0.3$) to 108

Table XI. Cycle Expansion for $w = 0.236$

n	# cycles	$p^{\phi}V$	D	λ	$\zeta(0,0)^{-1}$
2	24	0.5430	0.3769	1.4053	−0.4726
3	64	0.5588	0.3329	1.5082	−0.7028
4	108	0.8670	−0.0389	2.6829	−0.0918
5	252	−0.7384	1.7970	−3.2223	0.0762
6	716	0.7901	−0.0554	2.3036	0.0443
7	2184	0.6425	0.1821	1.8586	0.0212
8	5952	0.6236	0.2672	1.8515	−0.0052
9	19196	0.6426	0.2547	1.8661	−0.0093
10	51072	0.6969	0.2021	1.9664	0.0051
Direct	—	0.665(1)	0.1970(10)	—	—

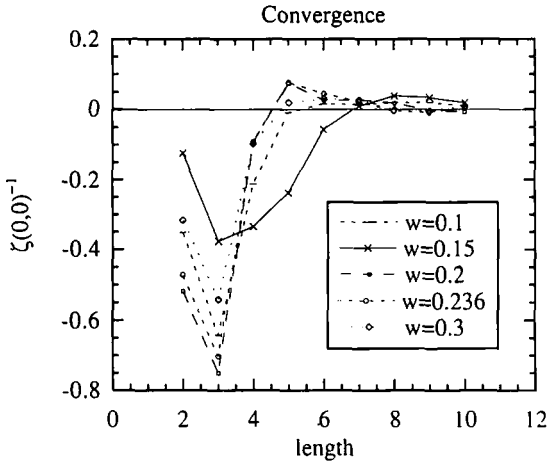

Fig. 9. The value of $\zeta(0,0)^{-1}$ as a function of length. This is a good estimate of the rate of convergence of the cycle expansions.

(at $w=0.236$); the number of prime length-5 UPOs has fallen from 516 (at $w=0.3$) to 252 (at $w=0.236$); and the number of prime length-6 UPOs has fallen from 1262 (at $w=0.3$) to 716 (at $w=0.236$). This leads to a change in the sign of the denominator of the cycle expansion [Eqs. (31) and (32)] at length 4 and hence to a negative value for the diffusion coefficient. Similar problems occur with the numerator of the pressure and Lyapunov exponent at length 5, and again with the diffusion coefficient at length 6. Despite these difficulties with smaller length cycles, the results at length 10 are significantly better, with the diffusion coefficient $\sim 2.5\%$ too high.

The relative convergence of the cycle expansion can be gauged by how close $\zeta(0,0)^{-1}$ is to zero. In Fig. 9 we plot $\zeta(0,0)^{-1}$ as a function of n for each state point. It can be seen that the convergence deteriorates with decreasing spacing w, which corresponds to an increase in the severity of cycle pruning. It would appear that as the level of pruning increases, the

Table XII. Pressure and Lyapunov Exponent

w	$p^{\phi}V$	$\langle p^{\phi}V\rangle_{\text{Shanks}}$	$\langle p^{\phi}V\rangle_{\text{cycle}}$	$\langle\lambda\rangle_{\text{Shanks}}$	$\langle\lambda\rangle_{\text{cycle}}$
0.1	1.163(1)	1.140(5)	1.20(10)	2.63(3)	2.66(9)
0.15	0.920(1)	0.907(4)	1.02(12)	2.31(3)	2.6(3)
0.2	0.751(1)	0.735(1)	0.73(4)	2.07(1)	1.99(8)
0.236	0.665(1)	0.69(5)	0.69(5)	1.94(2)	1.96(10)
0.3	0.5457(3)	0.54(2)	0.59(6)	1.76(2)	1.76(8)

Table XIII. Diffusion Coefficient

w	D_{Shanks}	D_{cycle}	D^*
0.100	0.090(4)	0.10(2)	0.0995(3)
0.150	0.139(4)	0.10(5)	0.1350(5)
0.200	0.176(5)	0.20(4)	0.170(1)
0.236	0.201(3)	0.20(5)	0.197(1)
0.300	0.243(9)	0.23(2)	0.2492(3)

cycle expansion convergence becomes worse and the POE is the preferred method.

In Tables XII and XIII we present a summary of the best estimates obtained for the pressure, Lyapunov exponent, and diffusion coefficient for each of the methods and state points considered. The periodic orbit expansion estimates are based on the Shanks transformation, while those for the cycle expansions are taken from the elementary cell calculations. In these tables the numbers in parentheses are the uncertainties in the last digit of

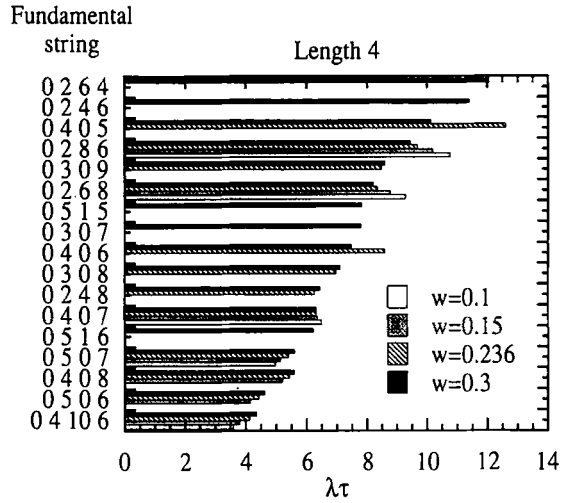

Fig. 10. For prime UPOs of length 4, the variation in $\lambda\tau$ with the spacing w for each of the symbol strings that is not pruned at $w = 0.3$. As the spacing decreases, more orbits are pruned, but there is no clear association between this pruning and the relative stabilities of the UPOs. $\Lambda_i^{-1} = \exp(-\lambda_i \tau_i)$. Also, the change in stability with spacing is an individual property of the UPO. For some orbits such as 0507, Λ_i^{-1} decreases with the increasing spacing, whereas for other orbits such as 0286 the reverse is true. The average Lyapunov exponent, however, decreases with increasing spacing as the behavior of more probable orbits (such as 0507) dominates the average.

the quoted result. The results $p^{\phi}V$ and D^* are those from Section 2. In all cases the uncertainty of the cycle expansion results are larger than those obtained from the POE using the Shanks transformation.

The pruning of prime UPOs with decreasing values of spacing w makes the cycle expansions less and less reliable as a means for calculating averages, while the periodic orbit expansions appear to be less affected, particularly when combined with the Shanks transformation. We can investigate the pruning of prime UPOs for orbits of small length. As the length increases, the number of UPOs increases and discussions about pruning become cumbersome. At length 2 there are four fundamental strings at $w=0.3$ and two as w approaches zero. The S and L orbits of Table II are always found. The T orbit exists for $w>0.1775$, while the V orbit is found for $w>0.21449$. In Section 4 we argued that the length-3 orbits could be considered as variations upon length-2 orbits. This would imply that the T′ orbit only exists while the T orbit exists, and similarly the V′ orbit would only exist while the V orbit exists. This would appear to be confirmed by the results we have presented. At length 4 the number of fundamental strings decreases from 17 at $w=0.3$ to 5 at $w=0.1$. In Fig. 10 we present the value of $\lambda\tau$ for each of the fundamental strings at each of the values of w. There are a number of observations we can make. The pruning with decreasing w is spread throughout the range of $\lambda\tau$ values as (0 2 8 6) appears for all values of w, while (0 5 1 6) is pruned before $w=0.236$. Also we note that for small values of $\lambda\tau$, $\lambda\tau$ decreases with decreasing w [for example, (0 4 0 8)] whereas for (0 2 6 8), $\lambda\tau$ increases with decreasing w.

8. CONCLUSIONS

The convergence of both the periodic orbit expansions and cycle expansions used here is not competitive with direct time averaging over the full chaotic trajectory as a means of calculating averages, even with the use of accelerating techniques. This is not surprising considering the fact that only a small fraction (about 1–2%) of the length of the chaotic trajectory is composed of approximate UPOs of length 10 or less. Despite this the average values for the diffusion coefficient, hydrostatic pressure, and Lyapunov exponent are all within about 8% of the correct values. The importance of these expansions is not in their use as a means of calculating thermodynamic averages, but that they give a direct method of developing approximations to the full phase space distribution function.

The calculation of the diffusion coefficient from a single very long trajectory, using either the mean square displacement or the Green–Kubo formula, was found to be very poor. The approach employed here of con-

sidering an ensemble of trajectories proves to be much more accurate, and systematic extrapolations in inverse time or in the inverse of the number of ensemble members provides very accurate results. The diffusion coefficient results obtained by in Section 2 are, we believe, the most accurate available.

Of the two expansion methods tested here the periodic orbit expansions based upon Eq. (8), combined with the Shanks transformation, are the most reliable. The cycle expansions based on the dynamical Ruelle ζ-function [Eq. (30)] are less accurate in the EC, and at best comparable in accuracy with the Shanks transformation results if carried out in the fundamental domain. It is not difficult to see the reasons for this. The development of the cycle expansions, by dividing the expansion into fundamental strings and curvature corrections, is designed to work best for systems with little or no pruning. In that case the curvature corrections approach zero with increasing length, and good results can be obtained. The Lorentz gas exhibits very strong pruning, and the degree of pruning depends upon the spacing w. The have shown that, for example, at $w = 0.236$, the mismatching of curvature corrections composed of length-4 strings minus products of length-2 strings can lead to very large errors. Indeed the average can even have the wrong sign. A second aspect of the mismatching of curvature corrections has to do with the degeneracies of the fundamental strings. This is a direct consequence of the symmetry of the Lorentz gas. We often observe that, for example, the curvature contribution associated with the symbol string (0 5 0 6), $t_{0506} - t_{05}t_{06}$, has different degeneracies associated with each of the two terms. The degeneracy of t_{0506} is 12, whereas the degeneracy of $t_{05}t_{06}$ is $12 \times 3 = 36$. This difference in degeneracy destroys any possibility of cancellation of curvature corrections.

The convergence of the periodic orbit expansions may often be improved by the Shanks transformation, but this is not always the case. The conditions under which the Shanks transformation is most usefully exploited is when the sequence shows strong oscillations with increasing length (in particular, when there is systematic deviation depending upon whether the length is even or odd). In the case where no even–odd effect is observed, one can rely on other conventional methods for the improvement of convergence (see ref. 22, for instance). The advantage of this approach is that the improvement in convergence is obtained at no extra computational cost, whereas the reduction to the fundamental domain is both formidable and not appropriate for some system properties (such as diffusion). Although the periodic orbit expansion can be formulated without the use of symbolic dynamics, we have found that symbolic dynamics techniques helps to enumerate all the possible UPOs, and, more importantly, for the Lorentz gas it explicitly builds in the symmetry, by the identification of the fundamental string and its degeneracy.

ACKNOWLEDGMENTS

We wish to thank P. Cvitanovic and T. Schreiber for a helpful correspondence with regard to the use of cycle expansions and symbolic dynamics. Thanks are in order to Eddie Cohen for suggesting the problem and for very stimulating and useful correspondence. This work has been supported by the Australian Research Council (A69131116) and GNFM-CNR (Italy). G.P.M. thanks the Research School of Chemistry, Australian National University, for providing the environment that initiated this work.

REFERENCES

1. D. J. Evans, E. G. D. Cohen, and G. P. Morriss, *Phys. Rev. A* **42**:5990 (1990).
2. P. Gaspard and S. A. Rice, *J. Chem. Phys.* **90**:2225, 2242, 2255 (1989).
3. J. Machta and R. Zwanzig, *Phys. Rev. Lett.* **50**:1959 (1983).
4. A. J. C. Ladd and W. G. Hoover, *J. Stat. Phys.* **38**:973 (1985); B. Moran and W. G. Hoover, *J. Stat. Phys.* **48**:709 (1987).
5. P. Gaspard and F. Baras, in *Microscopic Simulations of Complex Hydrodynamic Phenomena*, M. Mareschal and B. L. Holian, eds. (Plenum Press, New York, 1992).
6. N. I. Chernov, G. L. Eyink, J. L. Lebowitz, and Ya. G. Sinai, *Phys. Rev. Lett.* **70**:2209 (1993).
7. W. N. Vance, *Phys. Rev. Lett.* **69**:1356 (1992).
8. P. Cvitanovic, P. Gaspard and T. Schreiber, *Chaos* **2**:85 (1992).
9. D. J. Evans and G. P. Morriss, *Statistical Mechanics of Nonequilibrium Liquids* (Academic Press, London, 1990).
10. A. Baranyai, D. J. Evans, and E. G. D. Cohen, *J. Stat. Phys.* **70**:1085 (1993).
11. P. Cvitanovic, *Phys. Rev. Lett.* **61**:2729 (1988).
12. R. Artuso, E. Aurell, and P. Cvitanovic, *Nonlinearity* **3**:325, 361 (1990).
13. W. Parry, *Commun. Math. Phys.* **106**:267 (1986).
14. C. Grebogi, E. Ott, and J. A. Yorke, *Phys. Rev. A* **37**(5):1711 (1988).
15. D. Auerbach *et al.*, *Phys. Rev. Lett.* **58**:2387 (1987).
16. J. H. Hannay and A. M. Ozorio de Almeida, *J. Phys. A* **17**:3429 (1984).
17. P. Gaspard and D. Alonso Ramirez, *Phys. Rev. A* **45**:8383 (1992).
18. D. Ruelle, *Thermodynamic Formalism* (Addison-Wesley, Reading, Massachusetts, 1978).
19. P. Cvitanovic, Private communication.
20. P. Cvitanovic and B. Eckhardt, *Nonlinearity*, in press.
21. C. M. Bender and S. A. Orszag, *Advanced Mathematical Methods for Scientists and Engineers* (McGraw-Hill, New York, 1978).
22. W. H. Press *et al.*, *Numerical Recipes in C* (Cambridge University Press, Cambridge, 1988); G. Arfken, *Mathematical Methods for Physicists* (Academic Press, London, 1985).